buildings

MDPI

Article

Compressive Properties of Self-Compacting Concrete after Cooling from High Temperatures

Junru Zhu [1], Chuntao Zhang [2,*] and Wei Yu [3]

[1] School of Civil Engineering and Architecture, Southwest University of Science and Technology, Mianyang 621010, China
[2] Shock and Vibration of Engineering Materials and Structures Key Laboratory of Sichuan Province, Mianyang 621010, China
[3] College of Civil and Architecture Engineering, Guilin University of Technology, Guilin 541004, China
* Correspondence: chuntaozhang@swust.edu.cn

Abstract: Self-compacting concrete (SCC) has been widely used in building structures. However, previous research focused only on the mechanical properties and working properties of SCC at room temperature. Thus, there is limited research on the change of compressive strength of SCC after a fire. This paper aims to investigate the compressive properties of SCC after being cooled from high temperatures. The SCC specimens were firstly heated to a target temperature of 100–700 °C and were then cooled to ambient temperatures by water or in air. The heating and cooling damage to the SCC specimens was assessed by the mass loss and the ultrasonic pulse velocity (UPV) separately. Afterward, the axial compression tests were carried out to investigate the compressive properties of the fire-affected SCC specimens under uniaxial compression. The residual mass, UPV, stress–strain curves, post-fire failure characteristics, and compressive strengths of the SCC specimens were discussed in detail. The mass loss of the SCC specimens showed an obvious increase with the rising temperatures, while the UPV exhibited a converse pattern. The mass loss of the SCC specimens after being naturally cooled increased more significantly, while the two cooling methods used in this experiment had little effect on the UPV. When the SCC specimens were cooled from 100 °C, the compressive strength of the SCC specimens cooled in air or water dropped by 32.54% and 35.15%, respectively. However, while the heating temperature rose to 700 °C, the compressive strengths of the SCC specimens cooled in air or water dropped sharply by 72.98% and 86.51%, respectively. Finally, an improved mathematical model for SCC after cooling from high temperatures was proposed based on Jones and Nelson's equation. This improved material model matched the experimental results well, which demonstrates that the proposed constitutive model can provide better predictions for the SCC structures after a fire.

Keywords: self-compacting concrete; cooling methods; high temperatures; compressive properties; constitutive model

Citation: Zhu, J.; Zhang, C.; Yu, W. Compressive Properties of Self-Compacting Concrete after Cooling from High Temperatures. *Buildings* **2022**, *12*, 1875. https://doi.org/10.3390/buildings12111875

Academic Editor: Oldrich Sucharda

Received: 6 October 2022
Accepted: 1 November 2022
Published: 3 November 2022

1. Introduction

Concrete and steel are the most common construction materials in the world today. Because of the rapid development of infrastructures, the consumption of concrete and structural steel has been increasing in recent years [1,2], as shown in Figure 1. However, the application of conventional concrete has many disadvantages, such as complex construction processes, high construction noise, and long construction time. In recent years, the utilization of self-compacting concrete (SCC) has greatly attracted the interest of researchers and structural engineers. SCC, as a highly flowable type of concrete, is ideal to be used in drilled shafts, columns, and areas with a high concentration of rebar and pipes/conduits; it is placed and consolidated by means of its own weight without the need for mechanical vibration [3]. This not only strengthens the material properties of the concrete structural

members and shortens the construction time but also greatly improves the on-site working environment. According to the existing research results, SCC produces resistance to segregation by using mineral fillers or fines and using special admixtures, which have partially replaced cement in several nations [4–6]. These advantages enable SCC to be widely applied in tunnels, ultra-high-rise buildings, and long-span bridges [7–9]. However, structures are prone to fires, even though preventions such as coating have been applied. Recently, several fires have broken out in China, which partially devastated the high-rise structures in many cities and caused severe losses. In order to assess the residual bearing capacity of concrete structural members after a fire, it is critical to understand the residual mechanical properties of the fire-affected concrete that was cooled from high temperatures. In terms of compressive properties, the changes in elastic modulus, compressive strength, UPV, and mass loss are some of the most significant property parameters which need to be studied [10].

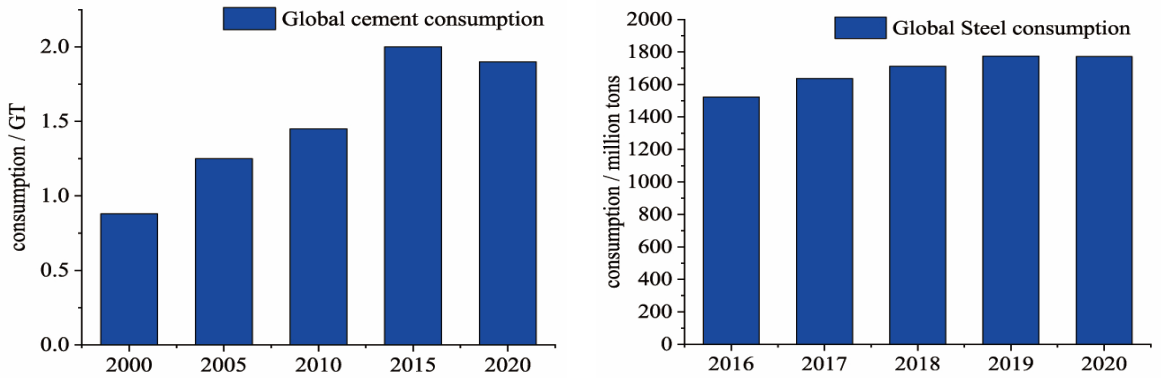

Figure 1. Consumption trends of global cement and steel.

Some researchers find that SCC, after being exposed to high temperature, shows a significant reduction in compressive strength and severe spalling behavior [11,12]. Compared with the previous studies on various steels after natural cooling [13,14], the compressive strength of SCC after being cooled from elevated temperatures also exhibited a similar decreasing trend. Several studies [11,15,16] have already noticed that the spalling probability of SCC is more pronounced than that of conventional concrete when exposed to rapidly increasing temperature fires. In general, because of its denser cementitious matrix, low-permeability concrete is more prone to cracking, which means that SCC is more sensitive to high temperatures than conventional concrete, and the degree of degradation varies with a range of parameters. Exposure temperature and duration, aggregate and cement used in the concrete, structural cross-sectional shape, geometry of concrete structural members, etc., are some of the influencing elements which affect the residual compressive behavior of concrete after being subjected to high temperatures [17].

In the case of heating and cooling, a series of physical reactions and chemical reactions typically take place in concrete, including the evaporation of void water, the disintegration of hydration products and aggregates, the phase transition of substances, and the increase of pores, which are considered to be the main reasons for the deterioration in the compressive properties of concrete after fires [18]. As for the deterioration, it can also be observed and analyzed from microscopic and mesoscopic perspectives [19]. In the existing studies, SCC meeting special combinations of performance and uniformity requirements that cannot always be achieved routinely by using conventional concrete is generally considered as high-performance concrete (HPC) [19–21]. Moreover, some remarkable conclusions showed that the mechanical properties of HPC, which can be obtained from the available bibliography [22,23]. When the HPC specimens were continuously heated in fires, because of the dense internal microstructure, the spalling gradually became severe, which made it difficult to transport and release the water vapor inside the concrete. Moreover, the compressive properties of HPC specimens were reduced much more rapidly than that of

conventional concrete. The mechanical properties of fire-affected concrete dropped with other aggregates have been investigated in detail [24,25]. These studies showed that the behavior of concrete in the fire was significantly affected by different aggregate types. In a study by Mehmet Burhan Karakoç, for instance, when the fine aggregate in concrete specimens was replaced with expanded perlite aggregate (EPA) and pumice aggregate (PA), the compressive strength of the concrete specimens that were cooled in water was much higher than that of the concrete specimens cooled in the air [24].

According to a literature survey, no sufficient information is available to understand the residual compressive behavior of SCC after being cooled by different cooling regimes. However, the SCC has gradually been applied in infrastructure construction. Because of the above statements, the residual mechanical properties of SCC specimens after being cooled from high temperatures using different cooling regimes are investigated in this present study. The SCC specimens were submitted to different temperature heating processes and were then cooled by different fire-extinguishing methods. After that, the specimens were submitted to compression tests. After the introduction of the experimental program and the testing process, the experimental results in terms of the mass loss, surface changing images, residual compressive strengths, the UPV, and the stress–strain relationship were extensively discussed. Finally, a new material model was presented which sheds new light for a clearer understanding of the relationship between the mechanical property and elevated temperatures of SCC with two different cooling regimes.

2. Experimental Program

2.1. Test Specimens

SCC specimens were prepared to investigate the relationship between materials properties, fire temperatures, and fire-extinguishing methods. The SCC with a nominal compressive strength of 35 MPa was selected as the test materials for the specimens. As for the cement, the type-I Portland Cement (PC42.5), known as common or general-purpose cement, was used in this experiment. The fine aggregate used for the concrete specimens was natural river sand with a fineness modulus of 3.0. Crushed gravel with a maximum size of 20 mm was used as coarse aggregate in all mixes. Table 1 provides the components and their corresponding proportions of the SCC used for the compressive specimens in this experiment.

Table 1. Components and corresponding proportions of the SCC specimens (kg/m^3).

Cement	Water	Sand	Coarse Aggregate	Fly Ash	Water Reducer	Silica Fume
380	140	770	910	180	16.2	40

In this study, the compression tests were performed using concrete cube tests. Hence, all specimens were designed as cubes with specific geometric dimensions of 150 mm × 150 mm × 150 mm. The water–cement ratio of the SCC used in this test was 0.37. The measured slump of the SCC in this test was 200 mm. Based on the guidelines provided in the Chinese National Standard (GB/T 50081-2019) [26], the SCC needed to be filled in the molds and cured in the required environment. The SCC specimens were first stored in moist air for 24 h. Then, the specimens were marked and removed from the molds and kept submerged in clear freshwater for 28 days [26]. Before testing, the SCC specimens with obvious defects or large geometric differences needed to be eliminated to ensure the accuracy of the test results.

2.2. Heating Procedure

For this study, the SCC specimens need to be heated and cooled prior to compression testing. An electric furnace that was capable of operating up to 2000 °C was used in this test. After the curing stage, the SCC specimens were heated to 100–700 °C with an internal

temperature of 100 °C. The heating rate of the SCC specimens in this test was 10 °C/min. Once the target temperature was reached, an exposure duration of 90 min was applied to ensure that the SCC specimens were heated uniformly, though this can further damage the materials properties of concrete [27]. To simulate the common firefighting methods, the heated SCC specimens were cooled in water or air prior to compression testing. In other words, some SCC specimens were naturally cooled in air, remaining in the furnace until the ambient temperature is reached; others were cooled in water, which means that these heated SCC specimens were taken out and then submerged in a huge water tank. The two cooling methods are shown in Figure 2.

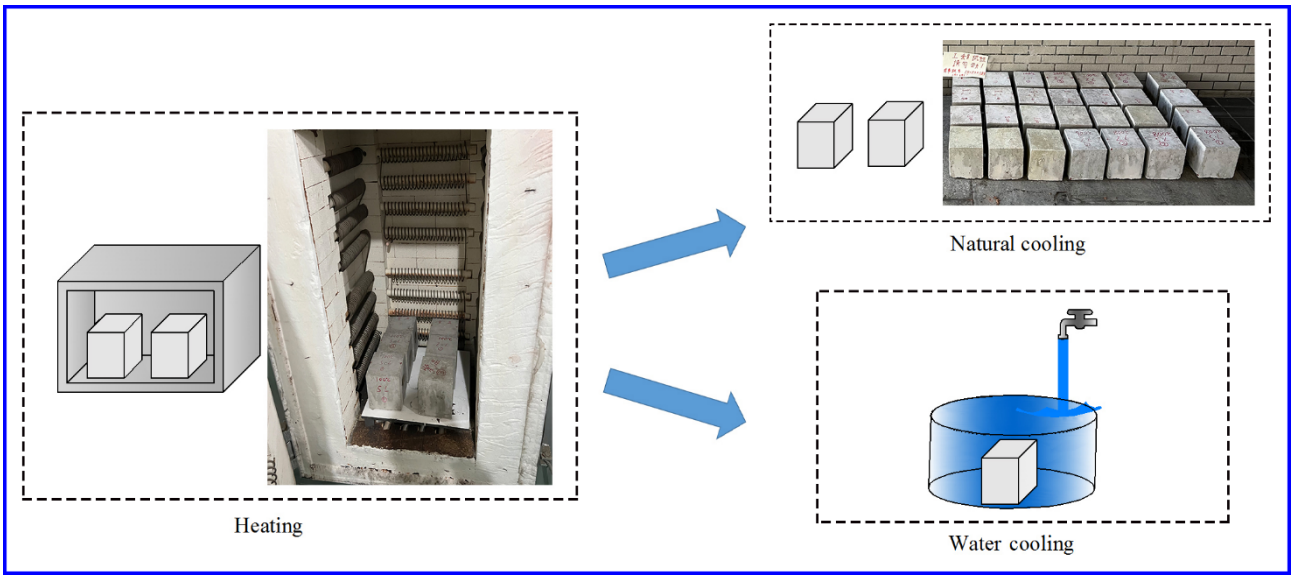

Figure 2. Heating and cooling of SCC specimens.

2.3. Test Procedures

The mass of each SCC specimen was measured by an electronic balance before and after heating and cooling, which can be used to calculate the mass loss rate by dividing the mass before the high temperature minus the mass after the high temperature by the mass before the high temperature due to fire and firefighting methods. Meanwhile, the UPV was also used to detect the damage to SCC specimens after the fire. Figure 3 presents the process of obtaining the UPV of the SCC specimens measured before and after the heating and cooling stages using an ultrasonic apparatus (RSM-SY5(T) Type). Each SCC specimen was tested three times to ensure the reliability of the measured data. The subsequent compression test was conducted with a displacement loading procedure with a loading rate of 0.5 mm/min. The compressive strength is obtained by a microcomputer-controlled electro-hydraulic servo pressure machine. Meanwhile, the test data were automatically collected and exported by computer. To ensure uniform compression, two steel plates were put on the upper and lower end faces of the SCC specimens before loading. In addition, in order to reduce and avoid the end-friction effect, it was necessary to apply a lubricant such as Vaseline on the upper and lower ends [28].

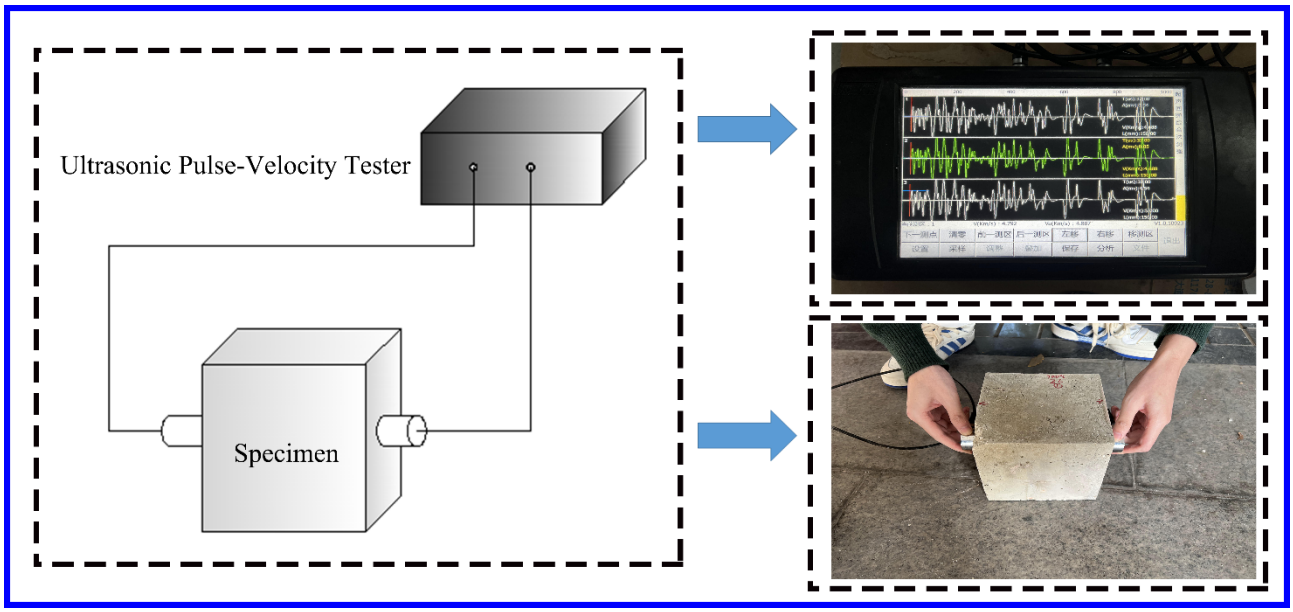

Figure 3. Ultrasonic pulse velocity measurement.

3. Test Results and Discussion

3.1. Visual Observation

Visual observation is beneficial for observing the most direct damage to the post-fire SCC specimens. Figures 4 and 5 show the air-cooled and water-cooled SCC specimens, respectively. Below 200 °C, the color of the SCC specimens subjected to elevated temperature and cooled by the two cooling regimes did not change much and remained greyish-white. After being cooled from 200 °C and 300 °C, the color of the water-cooled SCC specimens became slightly darker than that of the air-cooled SCC specimens, and some microcracks were formed on the surface of the heated and cooled SCC specimens. After being cooled from 400 °C, the crack width on the surface increased significantly, as shown in Figures 4e and 5e. The color of the SCC specimens cooled from 600 °C and 700 °C became more obvious, as shown in Figure 4g,h and Figure 5g,h. Meanwhile, after being cooled from 600 °C, the surface of the air-cooled SCC specimens was covered with cracks, which divided the surface of the SCC specimens into multiple polygonal areas. The surface of the water-cooled specimen was yellow-brown with cracks all over the surface. The edges and corners were seriously spalled, and the fine aggregates were exposed, which were greyish-white. When the exposure temperature was 700 °C, the SCC specimens cooled in air showed many yellow burst points, and the surface cracks propagated from the edges to the corners. The SCC specimens cooled using water were dark yellowish-brown, and the corners and the surface were severely spalled. Furthermore, compared to the air-cooled SCC cubes, more cracks can be observed on the water-cooled SCC cubes due to the increased internal stress which was caused by the dramatic change in temperature.

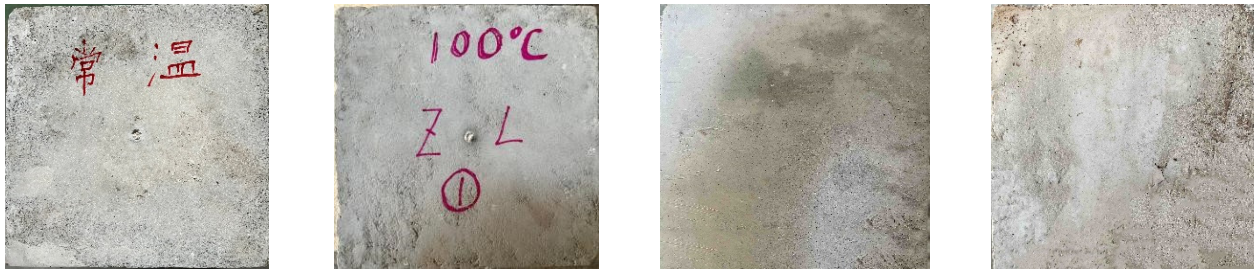

(**a**) 20 °C (**b**) 100 °C (**c**) 200 °C (**d**) 300 °C

(**e**) 400 °C (**f**) 500 °C (**g**) 600 °C (**h**) 700 °C

Figure 4. The surface of the SCC specimens cooled in air.

(**a**) 20 °C (**b**) 100 °C (**c**) 200 °C (**d**) 300 °C

(**e**) 400 °C (**f**) 500 °C (**g**) 600 °C (**h**) 700 °C

Figure 5. The surface of the SCC specimens cooled in water.

3.2. Mass Loss

After exposing the SCC specimens to elevated temperatures, the mass loss of the SCC specimens was measured. The mass loss of the specimen after heating and cooling was caused by the transportation of water and carbon dioxide. Table 2 provides the mass loss of each SCC specimen after heating and cooling. As anticipated, the mass loss of the SCC cubes exhibited an obvious increase with the heating temperature. The mass loss of the water-cooled SCC specimens was generally smaller than that of the air-cooled SCC specimens. The concrete cubes after being exposed to elevated temperatures have a higher water absorption capacity, which can erode the interior of the concrete. Therefore, the

compressive strength of the SCC specimen will be found to be affected in the subsequent analysis of the test results.

Table 2. Mass loss of SCC specimens after heating and cooling (%).

Cooling Regime (°C)	20	100	200	300	400	500	600	700
Air Cooling	0	0.66	3.97	6.08	7.20	8.41	10.87	12.83
Water Cooling	0	−0.41	1.26	2.33	2.25	2.63	5.43	8.48

3.3. Ultrasonic Pulse Velocity

For the concrete structures subjected to heating and cooling processes, testing the UPV is of high importance to evaluate the quality of the concrete. In general, the UPV changes of SCC specimens before and after heating and cooling can be used to evaluate the damage to the mechanical properties of the concrete specimens after a fire. The UPV was obtained by a UPV tester, as shown in Figure 3. Because of material transformation and crack formation inside the concrete, the time-history curve of the pulse speed changed significantly, as shown in Figure 6. Meanwhile, the UPV can be obtained from the time-history curve of the pulse speed, as shown Figure 7. The UPV of the SCC specimens cooled using two different cooling regimes in this study generally showed the same variation trend. It can be observed from Figure 7 that the UPV of SCC specimens can be reduced by increasing the exposure temperature. According to the UPV value in the previous study [29], the quality of the concrete can be classified into five grades, namely, the UPV values in the range of 0–2.14 km/s indicate the concrete is very poor; the UPV values in the range of 2.14–3.05 km/s indicate the concrete is poor; the UPV values in the range of 3.05–3.66 km/s indicate the concrete is questionable; the UPV values in the range of 3.66–4.58 km/s indicate the concrete is good; and the UPV values above 4.58 km/s indicate the concrete is excellent. The UPV value of the SCC specimens tested in this study was 4.73 km/s at room temperatures, which demonstrates that the quality of the SCC specimens used in this experiment was excellent at room temperatures. However, the UPV value of the SCC specimens cooled from 700 °C was only 1.3 km/s, which indicates that the SCC became very poor quality concrete. The UPV value of the SCC specimens after being cooled from 500 °C decreased significantly. However, the UPV values of the SCC specimens gradually decreased after being cooled from above 500 °C, which means that the internal cracking and material degradation of the SCC specimens were already severe.

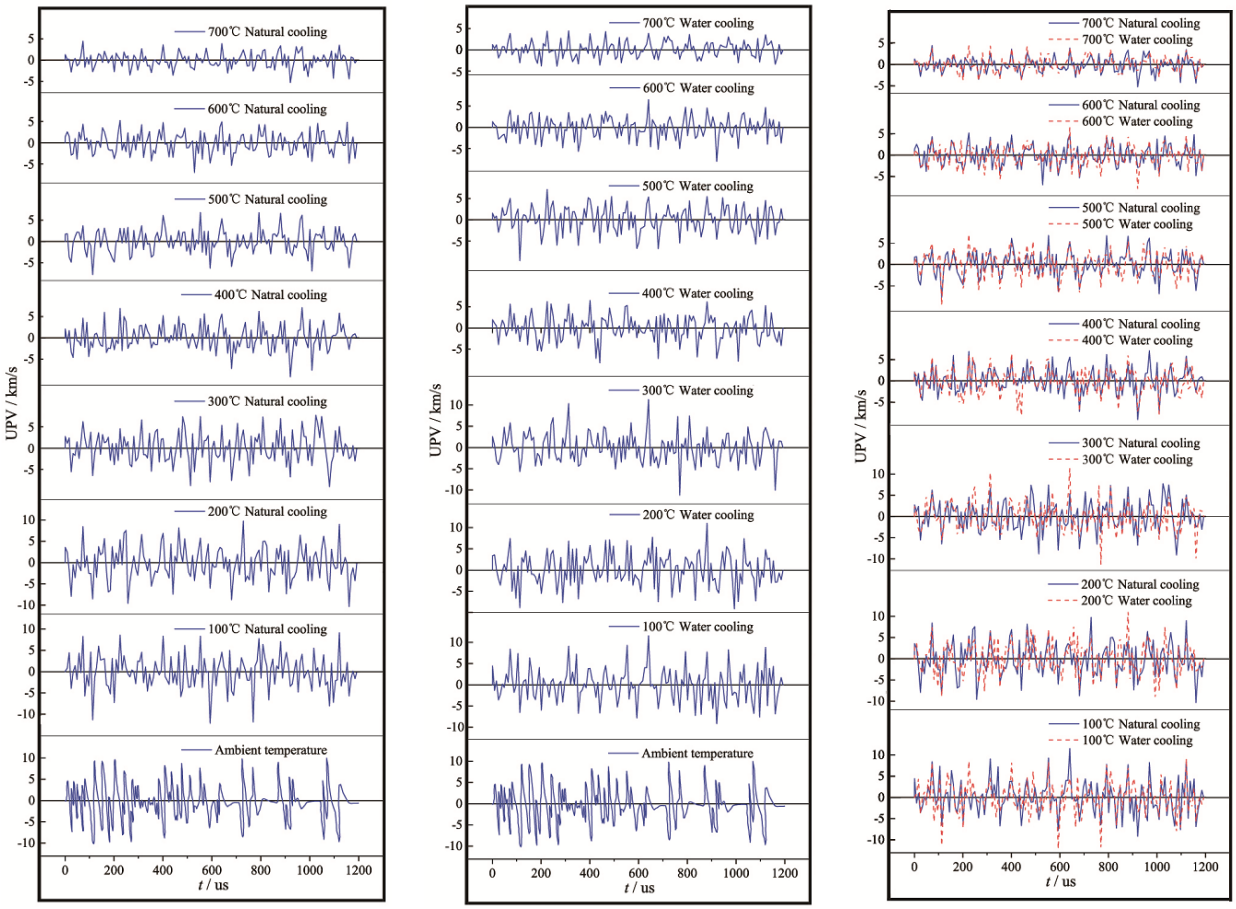

(**a**) Air cooling (**b**) Water cooling (**c**) Comparison

Figure 6. The velocity−time graphs of the SCC specimens after being heated and cooled.

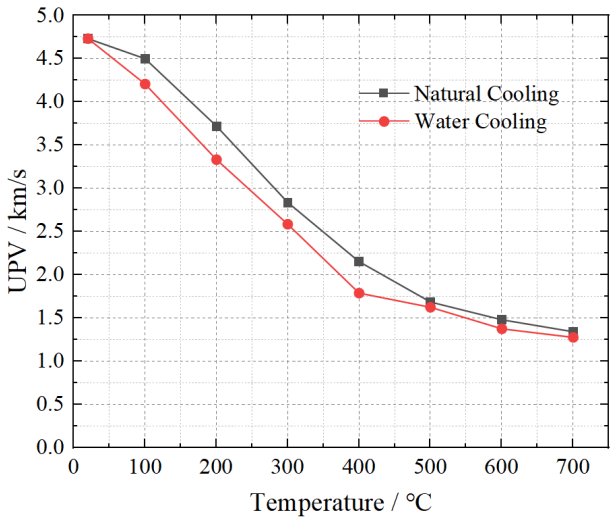

Figure 7. The UPV values of the SCC specimens after being cooled in water and air.

3.4. Compressive Strength

For the fire-affected SCC specimens, the compressive strengths obtained in this test are shown in Figure 8. An overall sharp drop in the compressive strength of the SCC specimens after being cooled in water can be observed. In the case of natural cooling, the compressive strength of the SCC specimens exhibited complex changes. After being

cooled from 100 °C in air and water, the compressive strengths of the fire-affected SCC specimens were 25.732 MPa and 24.738 MPa, respectively. The compressive strength of the undamaged SCC specimens was 38.15 MPa. Compared with the undamaged SCC specimens, the compressive strengths of the fire-affected SCC specimens after being cooled from 100 °C in air and water were reduced by 32.54% and 35.15%, respectively. According to the test data, it is worth noting that the reduction in compressive strength of SCC after being cooled from 100 °C was almost the same, and the effects of both air cooling and water cooling were negligible. By contrast, the compressive strength of the SCC specimens after being cooled using water from 100–400 °C still exhibited a reduction, whereas the reduction rate was significantly decreased. In the same cases, the compressive strength reduction of the air-cooled SCC specimens increased first and then decreased. When the SCC specimens were naturally cooled from 200 °C and 300 °C, the compressive strength decreased by 34.34% and 24.44%, respectively. When the temperature increased to 400 °C and 500 °C, the reduction in compressive strength of the air-cooled SCC specimens increased to 43.38% and 55.70%, respectively. After being cooled from 600 °C, the compressive strength of the air-cooled SCC specimens and the water-cooled SCC specimens decreased by 67.54% and 69.32%, respectively, with a difference of only 1.79%. It can be observed that the difference in the reduction rate of the compressive strength between the air-cooled SCC specimens and the water-cooled SCC specimens gradually became insignificant again. In this study, the SCC specimens after being cooled from the highest test temperature of 700 °C in water or air retained only 13.49% and 27.02% of their initial compressive strength, respectively.

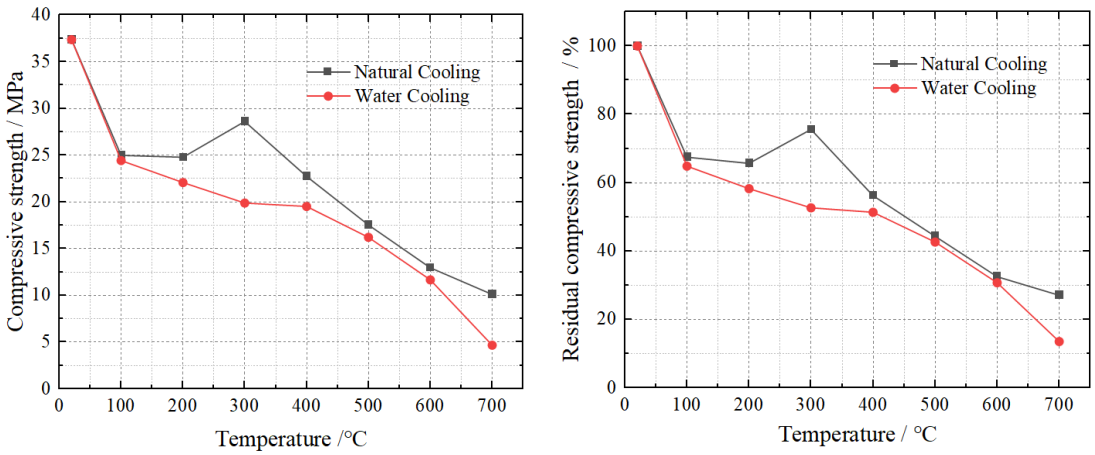

(**a**) Compressive strength (**b**) Residual factors

Figure 8. The compressive strength of SCC specimens after heating and cooling.

As for the SCC structures in the fire, it is easy to observe that the structural damage caused by extinguishing the fire with water is more serious than that caused by letting the fire naturally extinguish in the air. After the fire, the compressive strength of SCC dropped dramatically due to the loss of free water inside the concrete, which changed the hydrothermal conditions. In addition, the bonding force in C-S-H gel was weakened because of the dehydration and the decomposition of ettringite. When the fire temperature was low, the difference in the loss of free water and the weakening of the bonding force induced by the different fire-extinguishing methods was not obvious. When the temperature of the fire to which the SCC structures were subjected increased, the loss of free water and the weakening of the bonding force were different due to the different fire-extinguishing methods. As a result, the compressive strength of the SCC specimens after being cooled from 200 °C and 300 °C exhibited different changes due to the different extinguishing methods in this study. Moreover, when the temperature was 200 °C and 300 °C, the compressive strength of the air-cooled SCC specimens was higher than that of the water-cooled SCC specimens. The reason is that the C-S-H rehydration leads to water

migration and condensation in the cooler regions of the SCC specimens. In addition, the rehydration of the heated cement paste can be achieved by forming new C-S-H gels from new nesosilicates, which can be confirmed by the CaO/SiO_2 ratio approaching the original C-S-H gel and restoring its original stoichiometry [30]. When the SCC specimens were subjected to higher temperatures, the loss of free water and the weakening of the bonding force reached the limit value, and the different effects of various fire-extinguishing methods on the compressive strength of the SCC specimens were no longer obvious.

3.5. Stress–Strain Relationship

The data for plotting the stress–strain curve is calculated from the load–displacement curve which is obtained by the microcomputer-controlled electro-hydraulic servo pressure machine. In the case of natural cooling and water cooling, the compressive stress–strain curves of the SCC specimens after being cooled from temperatures of 100 °C to 700 °C are shown in Figures 9 and 10. For the heated and cooled SCC specimens, smoother stress–strain curves were produced as temperature increased. It can be seen from Figure 9a,b that the stress–strain curves of the SCC specimens cooled by the two different cooling methods show similar changes. As the temperature increased, the peak stress dropped sharply, whereas the ultimate strain increased sharply. Moreover, in the elastic phase, the slope of the curve decreased significantly, and the elastic modulus decreased with the increasing temperature. Except for 200 °C, the elastic modulus of the air-cooled specimens was greater than that of the water-cooled specimens. Both the SCC specimens that were cooled from 100–400 °C and the undamaged SCC specimens had similar stress–strain curves. The stress–strain curves of the SCC specimens after being cooled from the temperatures of 500–700 °C became slightly flat, indicating that the brittleness of the SCC specimens is reduced and the ductility is increased. Figure 10 shows the stress–strain curves of the SCC specimens after being cooled from temperatures of 100–800 °C by water or in air. The compressive strength of the air-cooled SCC specimens was greater than that of the water-cooled SCC specimens, which indicates that the damage to the SCC specimens cooled by water was greater than that of the SCC specimens cooled in air, regardless of the target temperature. This was related mainly to the sudden cooling of the SCC by water from the high temperature, and the extreme unevenness of internal and external temperatures led to the full development of structural damage and cracks in the concrete.

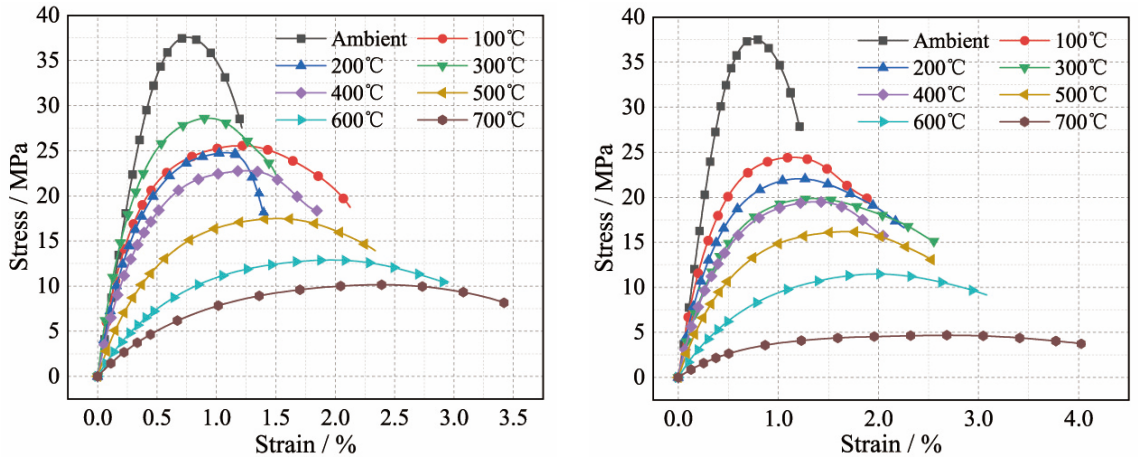

(**a**) Natural cooling (**b**) Water cooling

Figure 9. The stress–strain curves of the SCC specimens after cooling.

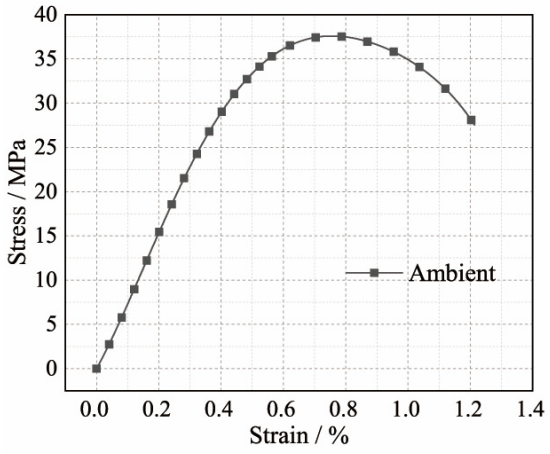

(**a**) 20 °C

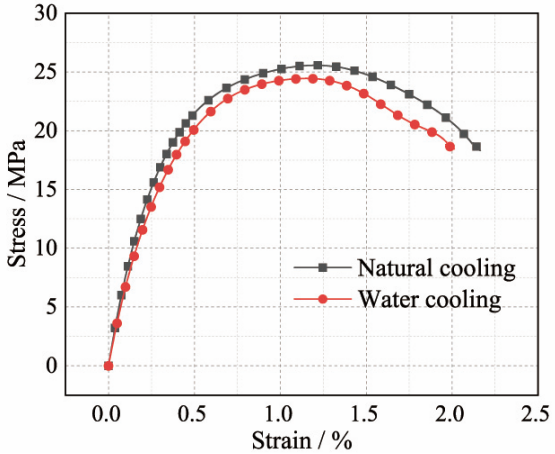

(**b**) 100 °C

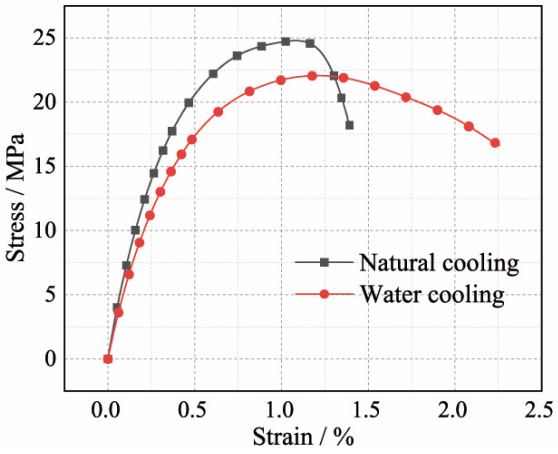

(**c**) 200 °C

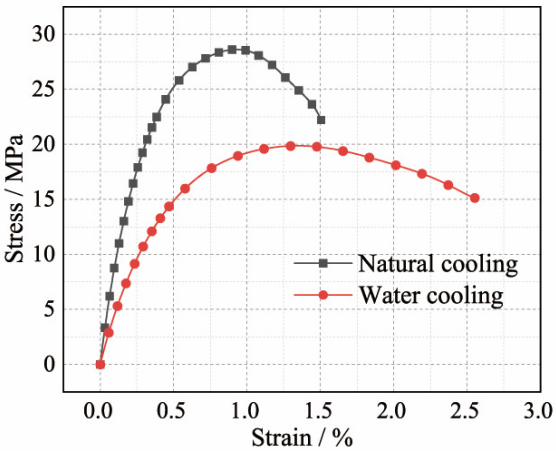

(**d**) 300 °C

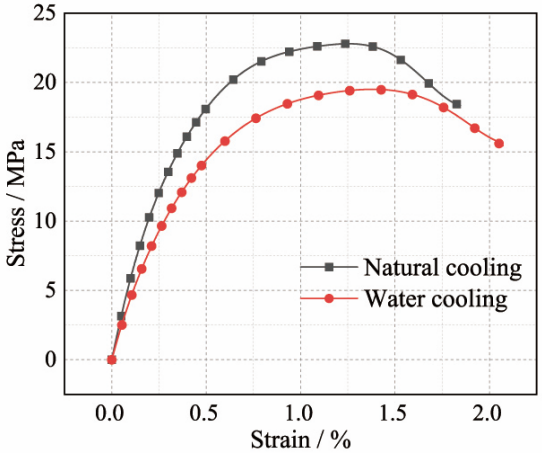

(**e**) 400 °C

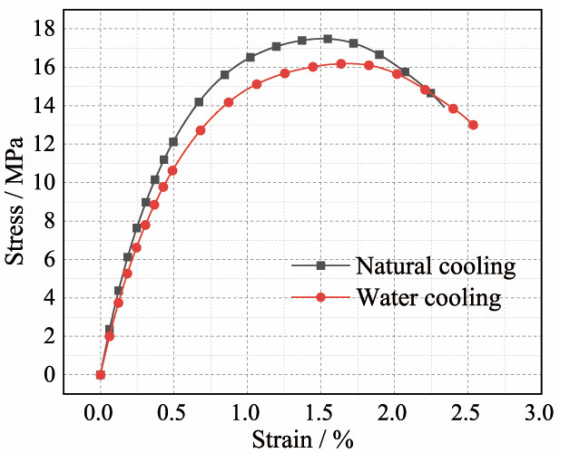

(**f**) 500 °C

Figure 10. *Cont.*

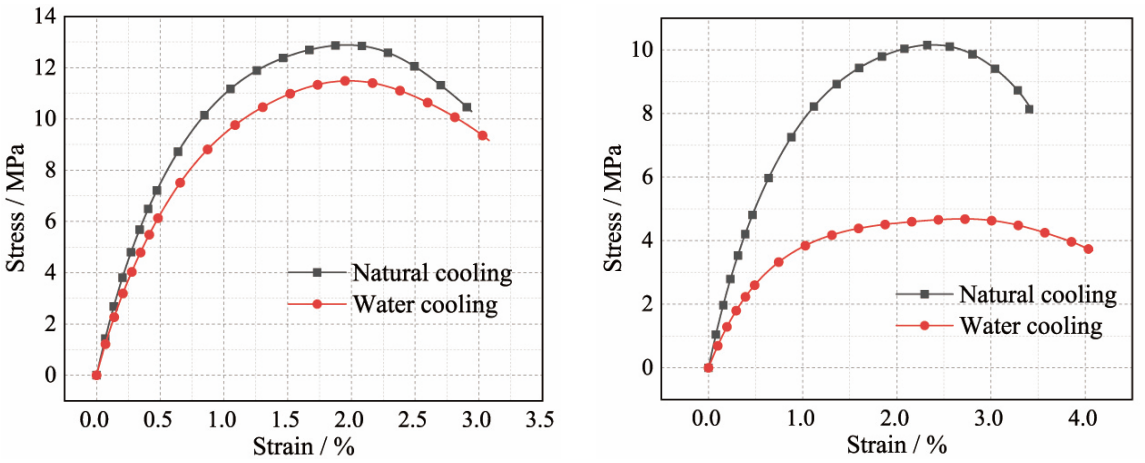

(**g**) 600 °C (**h**) 700 °C

Figure 10. The stress–strain curves of SCC specimens after water or natural cooling at each temperature.

4. Constitutive Model for Self-Compacting Concrete

4.1. Selection of the Basic Model Equation

A new material model, proposed by the Jones–Nelson model in previous studies [31–33] for the deformation behavior of ATS-J materials, is derived from the orthotropic plasticity theory. This material model can well describe the softening phenomenon of materials under axial loading. The most significant feature of the Jones–Nelson model is that the stress–strain relationship curve is characterized by the strain energy (U). The advantage of this is that a simple model can be implemented to analyze complex problems. Therefore, in this study, a nonlinear constitutive model of SCC is established by combining the Jones–Nelson model. The Jones–Nelson model is represented by the following equation:

$$Y_i = A_i \left[1 - B_i \left(\frac{U}{U_0} \right)^{C_i} \right] \tag{1}$$

where the material property Y is secant moduli, the parameter A represents the elastic value of the material property, B and C relate to the initial curvature and the rate of curvature respectively, and U is the strain energy density. i is the designation for one kind of material property. As described above, the constant A in Equation (1) is the elastic property. Therefore, the dimension of A can be considered as the dimension of the material property. U_0 represents a dimensionless ratio. Both U_0 and U own the same dimension of strain energy density. Before calculating the value of U_0, the values of B and C need to be determined. In Equation (1), both B and C are dimensionless. Hence, in the specific solution process, the values of B and C must be determined by the least-squares fit (regression analysis) method.

Taking Y as secant moduli ($E(\varepsilon)$), for example, the following shows how to obtain the values of the material model constants B and C. Then, Equation (1) can be expressed as:

$$E(\varepsilon) = A_i \left[1 - B_i \left(\frac{U}{U_0} \right)^{C_i} \right] \tag{2}$$

Transforming both sides of Equation (2), it can be expressed as:

$$B_i \left(\frac{U}{U_0} \right)^{C_i} = 1 - \frac{E(\varepsilon)}{A_i} \tag{3}$$

Taking the logarithm of both sides of Equation (3) can obtain:

$$\ln B_i + C_i \ln\left(\frac{U}{U_0}\right) = \ln\left(1 - \frac{E(\varepsilon)}{A_i}\right) \tag{4}$$

Let $x = \ln(U)$, $y = \ln\left(1 - \frac{E(\varepsilon)}{A_i}\right)$, and using the least-squares fitting method gives:

$$B_i = \frac{1}{\ln \frac{\sum y \sum (x^2) - \sum x \sum xy}{n\sum (x^2) - (\sum x)^2}} \tag{5}$$

$$C_i = \frac{n\sum (xy) - \sum x \sum y}{n\sum (x^2) - (\sum x)^2} \tag{6}$$

After the analysis in the above sections, the value ranges of B and C corresponding to the stress–strain curves of SCC specimens at ambient temperature can be effectively determined. The experimental curve and the calculated curve of the proposed constitutive model are compared in Figure 11. It can be observed that the calculated results show good agreement with the experimental results. The maximum difference between the experimental data and the calculated data is only 3%, not more than 5%. Therefore, the constitutive model equation, derived in this paper, can be well applied to the uniaxial compression properties of the SCC specimens.

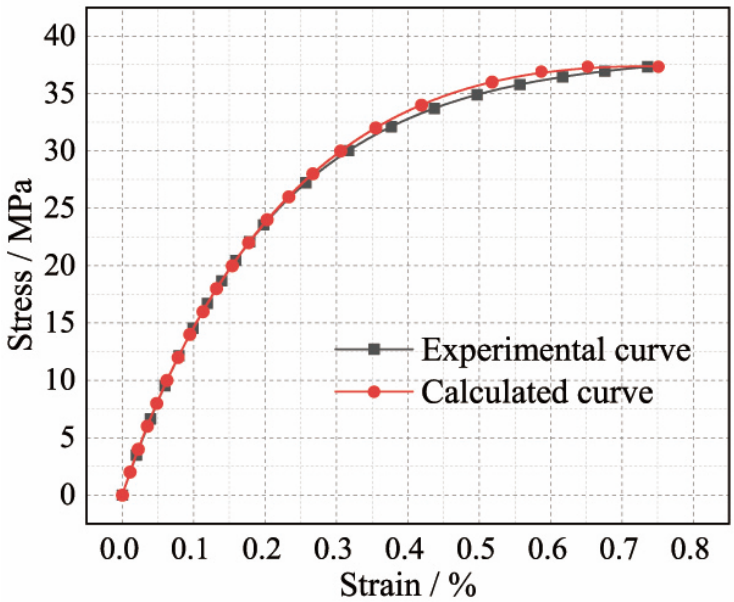

Figure 11. The comparison between the experimental compressive stress–strain curves and the calculated compressive stress–strain curves of the SCC.

4.2. Suggestion of the Model Equation

The nonlinear constitutive model of the SCC established in Section 4.1 is modified herein, and the temperature parameters and corresponding coefficients are imported. Therefore, the nonlinear constitutive model of the SCC after being exposed to elevated temperature can be modified as the following equation:

$$E(\varepsilon) = e^{-\alpha \Delta t} A_i \left[1 - B_i \left(\frac{U}{U_0}\right)^{C_i}\right] \tag{7}$$

where $\Delta t = T - (-273)$. According to the test data, for the naturally cooled specimens, α and Δt can be approximately fitted to a fifth-degree polynomial relationship, as shown in

Equation (8). For the water-cooled specimens, α and Δt can be approximately fitted to a third-degree polynomial relationship, as shown in Equation (9).

In the case of natural cooling:

$$E(\varepsilon) = e^{-\alpha\Delta t^5 + b\Delta t^4 - c\Delta t^3 + d\Delta t^2 - e\Delta t + f} A_i \left[1 - B_i \left(\frac{U}{U_0}\right)^{C_i}\right] \quad (8)$$

In the case of water cooling:

$$E(\varepsilon) = e^{-\alpha\Delta t^3 + b\Delta t^2 - c\Delta t + d} A_i \left[1 - B_i \left(\frac{U}{U_0}\right)^{C_i}\right] \quad (9)$$

On the basis of the experimental results and the proposed nonlinear constitutive model of the SCC, the material property constants and the model coefficients of the air-cooled SCC specimens are obtained, as listed in Table 3. The material property constants and the model coefficients of the water-cooled SCC specimens are listed in Table 4.

Table 3. The material property constants and the model coefficients of the air-cooled SCC specimens.

A_i	B_i	C_i	a	b	c	d	e	f
20,000	0.38233	0.347222	6.448×10^{-13}	-2.268×10^{-9}	3.097×10^{-6}	−4.03434	0.002038	77.62

Table 4. The material property constants and the model coefficients of the water-cooled SCC specimens.

A_i	B_i	C_i	a	b	c	d
20,000	0.38233	0.347222	2.69377×10^{-8}	-4.51329×10^{-5}	0.02617	−4.03434

4.3. Comparison of Experimental Curves and Established Constitutive Model

Figure 12 presents the experimental and predicted stress–strain curves of the fire-affected SCC specimens. In the case of the two fire-extinguishing methods, the calculated results of the proposed nonlinear constitutive model are generally in good agreement with the experimental results of the fire-affected SCC specimens. However, when the SCC specimens were cooled from 700 °C using water, notable differences in ultimate strain and peak stress can be observed between the calculated and experimental stress–strain curves, as shown in Figure 12n. Therefore, the constitutive model proposed in this study still needs to be further improved to describe the stress–strain curves of the SCC that were cooled from 700 °C using water.

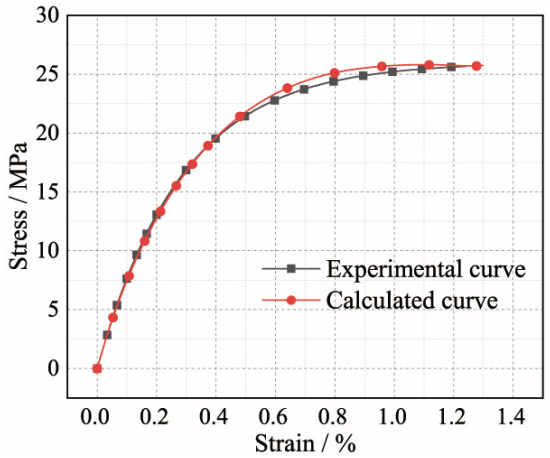

(**a**) T = 100 °C—Natural cooling

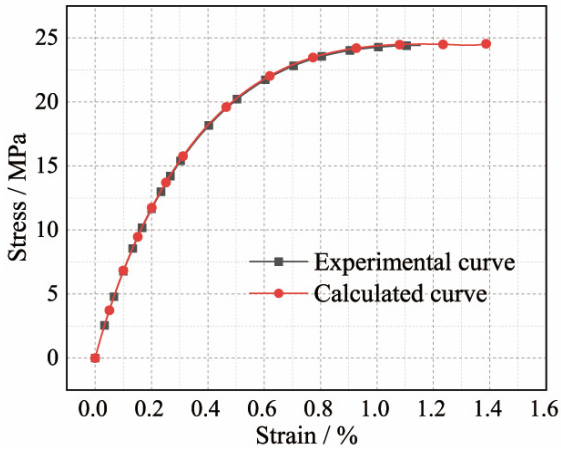

(**b**) T = 100 °C—Water cooling

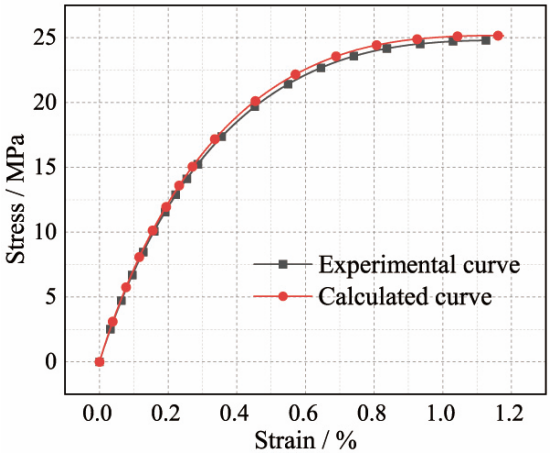

(**c**) T = 200 °C—Natural cooling

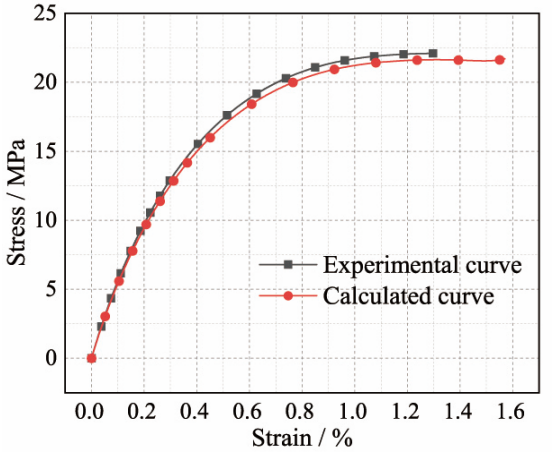

(**d**) T = 200 °C—Water cooling

Figure 12. *Cont.*

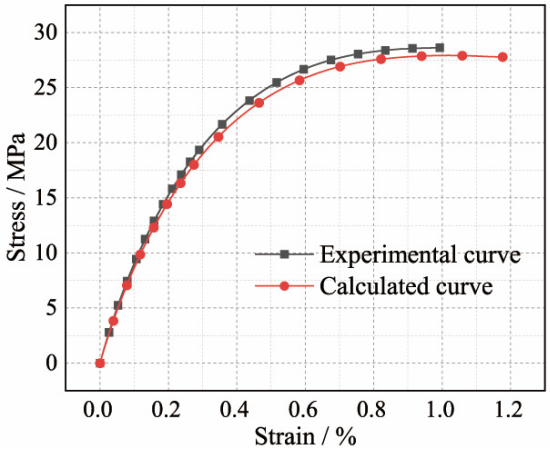

(**e**) T = 300 °C—Natural cooling

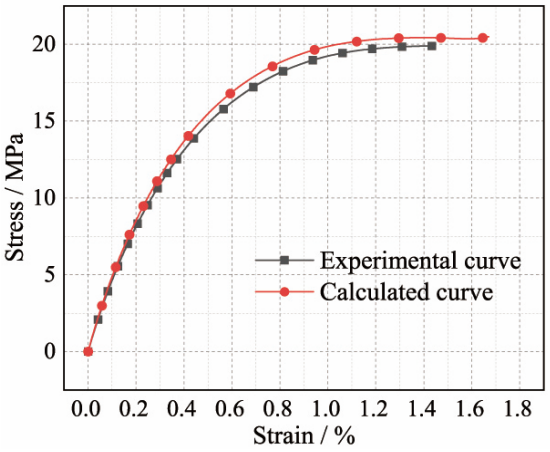

(**f**) T = 300 °C—Water cooling

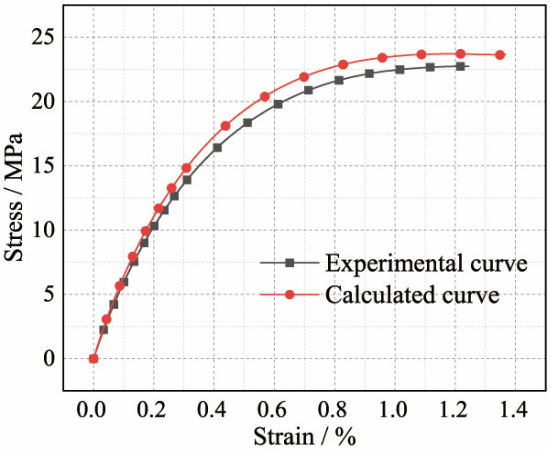

(**g**) T = 400 °C—Natural cooling

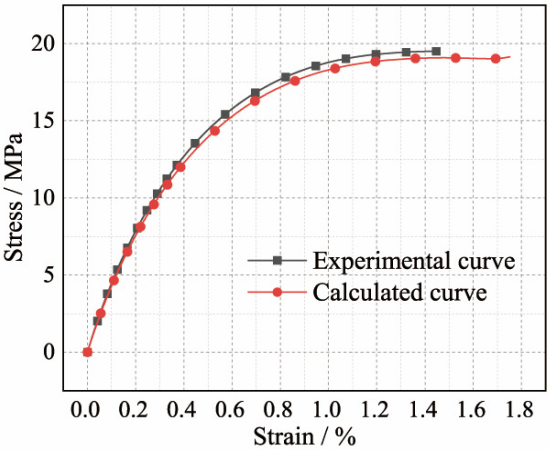

(**h**) T = 400 °C—Water cooling

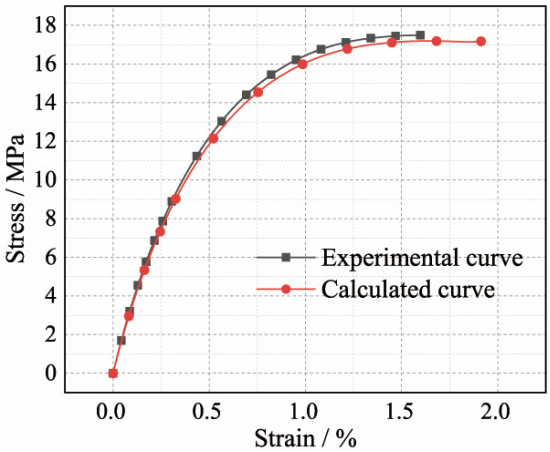

(**i**) T = 500 °C—Natural cooling

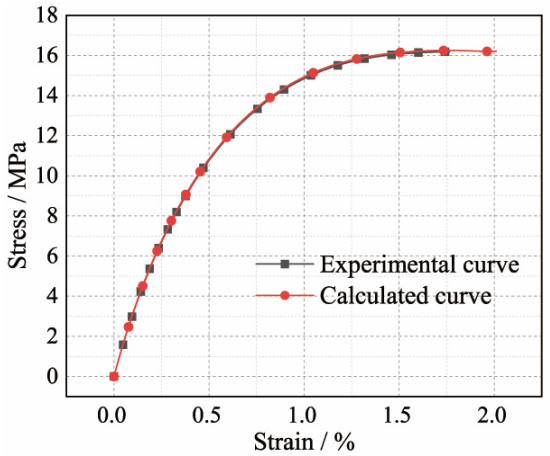

(**j**) T = 500 °C—Water cooling

Figure 12. *Cont.*

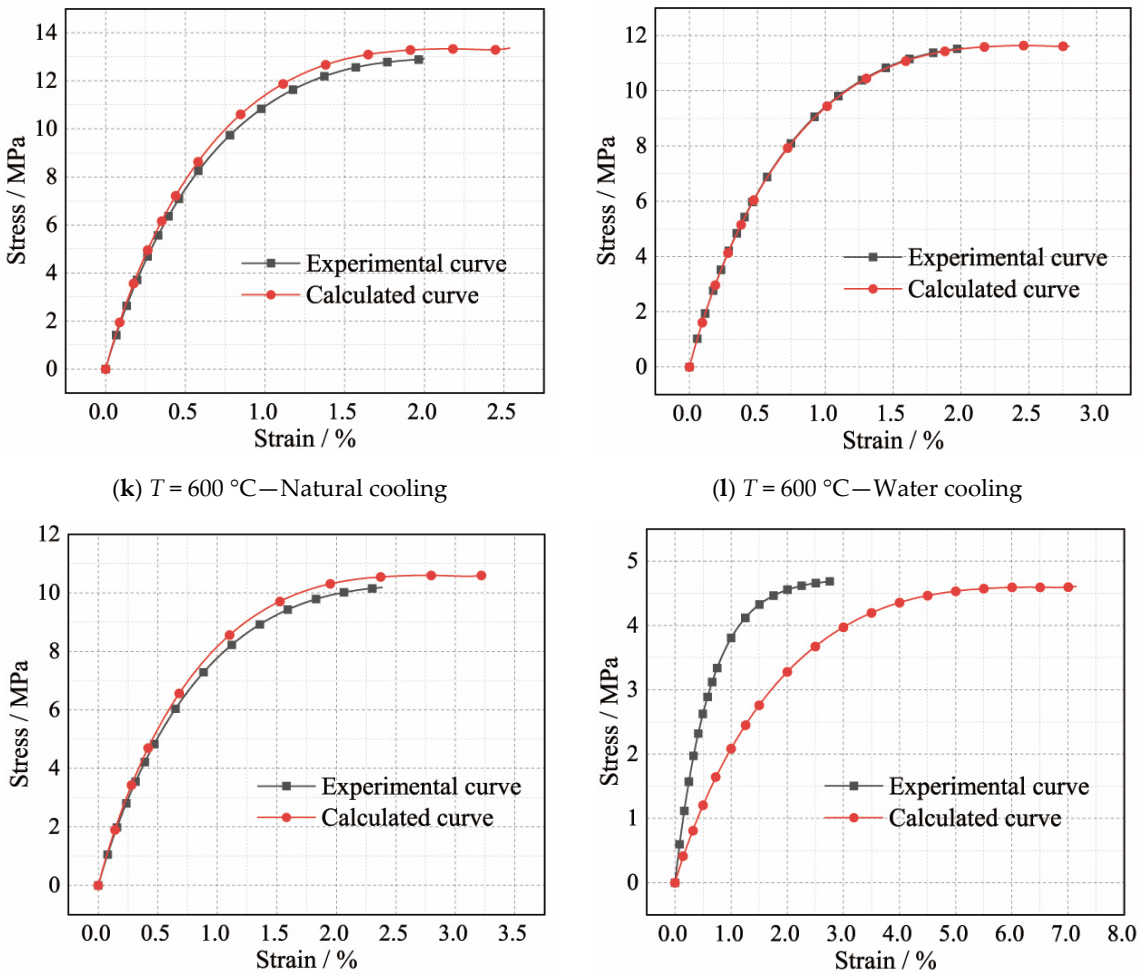

(**k**) T = 600 °C—Natural cooling (**l**) T = 600 °C—Water cooling

(**m**) T = 700 °C—Natural cooling (**n**) T = 700 °C—Water cooling

Figure 12. The comparison between experimental and calculated stress–strain curves of the fire-affected SCC.

5. Conclusions

For SCC that was cooled in water or air from a temperature range of 100–700 °C, the failure modes, residual compression properties, and the constitutive model were studied in this paper. The following key conclusions were obtained from the test results of the compression experiments and the calculated values of the proposed constitutive model.

1. Because of the different cooling rates, there was a huge temperature difference between the inside and outside of the SCC specimens. For the same SCC specimens, this temperature difference was different due to the different fire-extinguishing methods, which resulted in the internal expansion and external contraction of the SCC specimens. When the relative deformation between the inside and outside of the SCC specimens was large enough, many cracks appeared on the surface of the SCC specimens since the tensile stress exceeded the ultimate tensile strength of the concrete. Accordingly, the different failure modes of the air-cooled and water-cooled SCC specimens can be observed in this study. The different failure modes and compressive strengths of the SCC specimens were also due to the different internal and external temperature differences of the SCC specimens caused by the different fire-extinguishing methods.
2. Because of material transformation and crack formation inside the concrete, the time-history curve of the pulse speed changed significantly with the increase in temperature. However, the UPV of the SCC specimens cooled in water or air generally showed the

same variation trend. In other words, UPV cannot accurately evaluate the internal damage of the SCC specimens caused by different fire-extinguishing methods. The UPV of the SCC specimens gradually decreased after being cooled from above 500 °C, and the internal cracking as well as material degradation of the SCC specimens were already severe, and the quality of the corresponding SCC specimens became very poor.

3. Due to the loss of free water and the weakening of the bonding force, the compressive strength of the SCC specimens decreased significantly after being cooled from a temperature range of 100–700 °C. The compressive strength of the water-cooled SCC specimens dropped sharply, while the reduction in compressive strength of the air-cooled SCC specimens decreased first and then increased. For example, when the SCC specimens were naturally cooled from 200 °C and 300 °C, the compressive strength decreased by 34.34% and 24.44%, respectively; when the temperature increased to 400 °C and 500 °C, the reduction in compressive strength of the air-cooled SCC specimens increased to 43.38% and 55.70%, respectively. The SCC specimens after being cooled from the highest test temperature of 700 °C in water or air only retained 13.49% and 27.02% of their initial compressive strength, respectively.
4. The compressive stress–strain curves of the SCC cooled in water or air showed similar changes. When the temperature to which the SCC specimens were subjected increased, the peak stress dropped sharply, whereas the ultimate strain increased sharply. Meanwhile, the ascending phase of the compressive stress–strain curves became more linear, and the descending phase became flatter and smoother.
5. On the basis of the Jones–Nelson model, a nonlinear constitutive model of the SCC after being cooled by water or in air from high temperatures is proposed. The calculated results of the proposed nonlinear constitutive model are generally in good agreement with the experimental results of the fire-affected SCC specimens, where the proposed nonlinear constitutive model can be used to predict the compressive strength of the SCC after a fire.
6. Finally, because this study focused only on the compressive properties of C35 SCC after cooling from high temperatures, it is relatively limited. The authors hope that subsequent researchers can focus on other strength grades of SCC to meet the needs of different structural engineering. Additionally, by perfecting the Jones–Nelson constitutive model, the compressive properties of other strength grades of SCC after cooling from high temperatures can be predicted.

Author Contributions: J.Z. completed the experiment, processed the data, and programmed the iterative calculation of the Self-compacting concrete constitutive model. C.Z. guided and answered questions from the J.Z. throughout the trial. W.Y. provided guidance during the programming of the J.Z. All authors have read and agreed to the published version of the manuscript.

Funding: This research received no external funding.

Data Availability Statement: The data presented in this study are available on request from the corresponding author. The data are not publicly available due to [Fund Requirements].

Acknowledgments: This research work was supported by the National Natural Science Foundation of China (Grant No. 51868013, 51508482) and the Natural Science Foundation of Tibet Autonomous (Grant No. XZ202102YD0035C). The authors would like to express their sincere thanks for their support.

Conflicts of Interest: The authors declare no conflict of interest.

References

1. Dong, J.F.; Wang, Q.Y.; Guan, Z.W. Material properties of basalt fibre reinforced concrete made with recycled earthquake waste. *Constr. Build. Mater.* **2017**, *130*, 241–251. [CrossRef]
2. Zhang, C.T.; Gong, M.Q.; Zhu, L. Post-fire mechanical behavior of Q345 structural steel after repeated cooling from elevated temperatures with fire-extinguishing foam. *J. Constr. Steel. Res.* **2022**, *191*, 107201. [CrossRef]

3. Tayyeb, A.; Shazim, A.M.; Humayun, O. Production of low cost self-compacting concrete using bagasse ash. *Constr. Build. Mater.* **2008**, *23*, 703–712.
4. Kapoor, M.E.K.; Singh, S.P.; Singh, B. Durability of self-compacting concrete made with Recycled Concrete Aggregates and mineral admixtures. *Constr. Build. Mater.* **2016**, *128*, 67–76. [CrossRef]
5. European Federation for Specialist Construction Chemicals and Concrete Systems (EFNARC). *Specification and Guidelines for Self-Compacting Concrete*; European Federation of National Associations Representing Producers and Applicators of Specialist Building Products for Concrete (EFNARC): Norfolk, UK, 2002; p. 32.
6. Younes, O.; Benchaa, B.; Rajab, A.; El-Hadj, K.; Jamal, K. Effect of using metakaolin as supplementary cementitious material and recycled CRT funnel glass as fine aggregate on the durability of green self-compacting concrete. *Constr. Build. Mater.* **2020**, *235*, 117802.
7. Li, B.; Wu, C.; Li, Y.; Wang, S.N.; Jia, L.L.; Xia, D.T. Expansive behavior of high-strength self-stressing and self-compacting concrete: Experimental study and analytical model. *Constr. Build. Mater.* **2022**, *353*, 129080. [CrossRef]
8. Wu, M.M.; Xing, X.; Shen, W.G.; Huo, X.J.; Xue, G.L.; Zhang, B.L.; Li, J.W.; Zhang, W.S. Material design and engineering application of Fair-faced self-compacting concrete. *Constr. Build. Mater.* **2021**, *300*, 123992. [CrossRef]
9. Dushimimana, A.; Niyonsenga, A.A.; Nzamurambaho, F. A review on strength development of high performance concrete. *Constr. Build. Mater.* **2021**, *307*, 124865. [CrossRef]
10. Pathak, N.; Siddique, R. Effects of elevated temperatures on properties of self-compacting concrete containing fly ash and spent foundry sand. *Constr. Build. Mater.* **2012**, *34*, 512–521. [CrossRef]
11. Sideris, K.K.; Manita, P. Residual mechanical characteristics and spalling resistance of fiber reinforced self-compacting concretes exposed to elevated temperatures. *Constr. Build. Mater.* **2013**, *41*, 296–302. [CrossRef]
12. Mohammed, A.; de Jorge, B. Evaluation of high-performance self-compacting concrete using alternative materials and exposed to elevated temperatures by non-destructive testing. *J. Build. Eng.* **2020**, *32*, 101720.
13. Zhang, C.T.; Zhu, H.J.; Zhu, L. Effect of interaction between corrosion and high temperature on mechanical properties of Q355structural steel. *Constr. Build. Mater.* **2021**, *271*, 121605. [CrossRef]
14. Zhang, C.T.; Wang, R.H.; Zhu, L. Mechanical properties of Q345 structural steel after artificial cooling from elevated temperatures. *J. Constr. Steel. Res.* **2021**, *176*, 106432. [CrossRef]
15. Liu, X.; Ye, G.; Schutter, G.D.; Yuan, Y.; Taerwe, L. On the mechanism of polypropylene fibres in preventing fire spalling in self-compacting and high-performance cement paste. *Cement Concr. Res.* **2008**, *38*, 487–499. [CrossRef]
16. Annerel, E.; Taerwe, L.; Vandevelde, P. Assessment of temperature increase and residual strength of SCC after fire exposure. In Proceedings of the 5th international RILEM symposium on SCC, Ghent, Belgium, 3–5 September 2007; pp. 715–720.
17. Mahdi, R.; Mohd, R.S.; Jahangir, M.; Mohd, W.H.; Salmiati, R.K.; Rawid, K.; Elnaz, K. Toxicity characteristics and durability of concrete containing coal ash as substitute for cement and river sand. *Constr. Build. Mater.* **2017**, *143*, 234–246.
18. Ma, Q.M.; Guo, R.X.; Zhao, Z.M.; Lin, Z.W.; He, K.C. Mechanical properties of concrete at high temperature—A review. *Constr. Build. Mater.* **2015**, *93*, 371–383. [CrossRef]
19. Yu, Z.; Ding, D.; Bi, J.; Wang, C.L.; Liu, P.F. Experimental study on mechanical properties of precast cracked concrete under different cooling methods. *Constr. Build. Mater.* **2021**, *301*, 124141.
20. Omer, A. Effects of elevated temperatures on properties of concrete. *Fire Saf. J.* **2007**, *42*, 516–522.
21. Wu, Y.P.; Wu, B. Residual compressive strength and freeze-thaw resistance of ordinary concrete after high temperature. *Constr. Build. Mater.* **2014**, *54*, 596–604. [CrossRef]
22. Kaczmarczyk, G.P.; Wałach, D.; Natividade-Jesus, E.; Ferreira, R. Change of the Structural Properties of High-Performance Concretes Subjected to Thermal Effects. *Materials* **2022**, *16*, 5773. [CrossRef]
23. Monte, F.L.; Felicettia, R.; Miah, M.J. The influence of pore pressure on fracture behaviour of Normal-Strength and High-Performance Concretes at high temperature. *Cement. Concrete. Comp.* **2019**, *104*, 103388. [CrossRef]
24. Mehmet, B.K. Effect of cooling regimes on compressive strength of concrete with lightweight aggregate exposed to high temperature. *Constr. Build. Mater.* **2013**, *41*, 21–25.
25. Larissa, C.D.A.; dos Anjos, M.A.; de Sá, M.V.; de Souza, N.S.; de Farias, E.C. Effect of high temperatures on self-compacting concrete with high levels of sugarcane bagasse ash and metakaolin. *Constr. Build. Mater.* **2020**, *248*, 118715.
26. *GB/T 50081-2019*; UDC, Standard for Test Methods of Concrete Physical and Mechanical Properties. Ministry of Housing and Urban-Rural Development of the People's Republic of China, and General Administration of Quality Supervision: Beijing, China, 2019.
27. Cheng, Z.H.; Lu, J.; Liu, H.B.; Liao, X.W. Experimental study on the post-fire mechanical properties of high-strength steel tie rods. *J. Constr. Steel Res.* **2016**, *121*, 311–329. [CrossRef]
28. Li, B.B.; Xiong, H.B.; Jiang, J.F. End-Friction Effect on Concrete Cubes with Passive Confinement. *J. Mater. Civil. Eng.* **2018**, *8*, 04018194. [CrossRef]
29. Solís-Carcaño, R.; Moreno, E.I. Evaluation of concrete made with crushed limestone aggregate based on ultrasonic pulse velocity. *Constr. Build. Mater.* **2007**, *22*, 1225–1231. [CrossRef]
30. Alonso, C.; Fernandez, L. Dehydration and rehydration processes of cement paste exposed to high temperature environments. *J. Mater. Sci.* **2004**, *39*, 3015–3024. [CrossRef]

31. Jones, R.M.; Nelson, D.A.R. A New Material Model for the Nonlinear Biaxial Behavior of ATJ-S Graphite. *J. Compos. Mater.* **1975**, *9*, 10–27. [CrossRef]
32. Jones, R.M. Further Characteristics of a Nonlinear Material Model for ATJ-S Graphite. *J. Compos. Mater.* **1975**, *9*, 251–265. [CrossRef]
33. Jones, R.M.; Nelson, D.A.R. Material Models for Nonlinear Deformation of Graphite. *AIAA J.* **1976**, *14*, 709–717. [CrossRef]